



# 4D-Flow MRI intracardiac flow analysis considering different subtypes of pulmonary hypertension

Michael T. Cain<sup>1</sup>  | Michal Schäfer<sup>1</sup>  | Lexie K. Ross<sup>2</sup> | David D. Ivy<sup>2</sup> |  
Max B. Mitchell<sup>2</sup> | Brett E. Fenster<sup>3</sup> | Todd M. Bull<sup>4</sup> | Alex J. Barker<sup>5</sup> |  
Daniel Vargas<sup>5</sup> | Jordan R. H. Hoffman<sup>1</sup>

<sup>1</sup>Division of Cardiothoracic Surgery, Anschutz Medical Campus, University of Colorado Denver, Aurora, Colorado, USA

<sup>2</sup>Division of Pediatric Cardiology, Children's Hospital Colorado, Anschutz Medical Campus, University of Colorado Denver, Aurora, Colorado, USA

<sup>3</sup>Division of Cardiology, Colorado Kaiser Permanente Medical Group, Denver, Colorado, USA

<sup>4</sup>Department of Critical Care and Pulmonary Medicine, Anschutz Medical Campus, University of Colorado Denver, Aurora, Colorado, USA

<sup>5</sup>Department of Radiology, Anschutz Medical Campus, University of Colorado Denver, Aurora, Colorado, USA

## Correspondence

Michal Schäfer, Division of Cardiothoracic Surgery, Anschutz Medical Campus, University of Colorado, 13123 E 16th Ave, Aurora, CO 80045-2560, USA.

Email: [Michal.schafer@cuanschutz.edu](mailto:Michal.schafer@cuanschutz.edu)

## Funding information

Rady Family and Jayden DeLuca foundations

## Abstract

Intracardiac flow hemodynamic patterns have been considered to be an early sign of diastolic dysfunction. In this study we investigated right ventricular (RV) diastolic dysfunction between patients with pulmonary arterial hypertension (PAH) and pulmonary hypertension with chronic lung disease (PH-CLD) via 4D-Flow cardiac MRI (CMR). Patients underwent prospective, comprehensive CMR for function and size including 4D-Flow CMR protocol for intracardiac flow visualization and analysis. RV early filling phase and peak atrial phase vorticity (E-vorticity and A-vorticity) values were calculated in all patients. Patients further underwent comprehensive Doppler and tissue Doppler evaluation for the RV diastolic dysfunction. In total 13 patients with PAH, 15 patients with PH-CLD, and 10 control subjects underwent the 4D-Flow CMR and echocardiography evaluation for RV diastolic dysfunction. Reduced E-vorticity differentiated PAH and PH-CLD from healthy controls (both  $p < 0.01$ ) despite the same Doppler E values. E-vorticity was further decreased in PAH patients when compared to PH-CLD group ( $p < 0.05$ ) with similar Doppler and tissue Doppler markers of diastolic dysfunction. A-vorticity was decreased in both PAH and PH-CLD groups compared to controls but with no difference between the disease groups. E-vorticity correlated with ejection fraction ( $R = 0.60$ ,  $p < 0.001$ ), end-systolic volume ( $R = 0.50$ ,  $p = 0.001$ ), stroke volume ( $R = 0.42$ ,  $p = 0.007$ ), and cardiac output ( $R = 0.30$ ,  $p = 0.027$ ). Intracardiac flow analysis using 4D-Flow CMR derived vorticity is a sensitive method to differentiate diastolic dysfunction in patients with different PH etiology and similar Doppler echocardiography profile.

## KEYWORDS

4D-Flow MRI, diastolic dysfunction, pulmonary hypertension, right ventricle, vorticity

This is an open access article under the terms of the Creative Commons Attribution-NonCommercial License, which permits use, distribution and reproduction in any medium, provided the original work is properly cited and is not used for commercial purposes.

© 2023 The Authors. *Pulmonary Circulation* published by John Wiley & Sons Ltd on behalf of Pulmonary Vascular Research Institute.

## INTRODUCTION

Idiopathic pulmonary arterial hypertension (PAH or PH-Type I) and pulmonary hypertension due to chronic lung disease or hypoxia (PH-CLD or PH-Type III) arise from different pathophysiologic processes, yet they both culminate in increased right ventricular (RV) afterload and eventual RV failure.<sup>1,2</sup> While the clinical presentation and history can substantially differ between the two groups, the initial signs of right heart systolic and diastolic dysfunction on screening echocardiography can be indistinguishable.<sup>3,4</sup> Furthermore, right heart catheterization in both groups yields hemodynamic profile resembling pre-capillary pulmonary hypertension. Cardiac MRI (CMR) is arguably the most comprehensive method to assess accurate quantitative hemodynamics of cardiopulmonary vascular unit.<sup>5</sup> However, the initial attempts to phenotype PH subgroups based on standard CMR indices of bi-ventricular size and function have shown that CMR can only reliably hemodynamically distinguish PAH from other subtypes.<sup>6</sup>

Intracardiac flow hemodynamic patterns have been considered to be an early biomarker to characterize and detect signs of diastolic dysfunction with the mechanistic premise that changes in the ventricular flow domain would be detectable sooner than early stage of myocardial tissue remodeling resulting in loss of elastic recoil.<sup>7,8</sup> Historically, 4D-Flow CMR has shown great potential to phenotype and differentiate biventricular pathologies based on qualitative and quantitative intracardiac flow patterns.<sup>9–11</sup> Furthermore, multiple studies indicated that 4D-Flow CMR outperforms Doppler and Tissue Doppler indices in characterization of RV-pulmonary axis and ventricular function.<sup>12,13</sup> Given the potential bias associated with qualitative flow grading schemes and complexity of the RV geometry, 4D-Flow CMR vorticity analysis has emerged as a quantitative tool to characterize RV systolic and diastolic flow patterns.<sup>10,14</sup> Vorticity is defined as a local spinning motion of an element of fluid and has been hypothesized to be a sensitive measure of vortex dynamics. As fluid dynamic marker vorticity is determined by 3-dimensional velocity vector field and surface along which it has been formed. Therefore, it interconnects flow hemodynamic parameters reflective of preload and cardiac structural morphology.

We sought to investigate RV intracardiac flow patterns in patients with PAH and PH-CLD via 4D-Flow CMR. Specifically, we hypothesized that 4D-Flow CMR inflow diastolic vorticity will be different between the PH groups. To address this hypothesis, we aimed to evaluate RV inflow diastolic vorticity between these two PH groups and a healthy control group. Considered imaging markers included 4D-Flow MRI derived

vorticity and standard Doppler and tissue-Doppler markers of diastolic dysfunction. We further sought to correlate RV vorticity with standard right heart catheterization hemodynamics and standard echocardiographic markers of the RV diastolic dysfunction.

## METHODS

This was a prospective, single-institution, cohort study of patients with previously diagnosed PH who underwent a comprehensive CMR protocol including the 4D-Flow MRI evaluation. All enrolled patients have met the PH criteria (mean pulmonary arterial pressure [mPAP] >20 mmHg) on prior right heart catheterization and were categorized into PAH or PH-CLD groups based on clinical presentation, history, and additional imaging-based evaluation, including chest CT, and cardiopulmonary exercise tests as clinically indicated individual basis. All patients underwent clinically indicated echocardiography within 6 months of their CMRI study. Exclusion criteria included age <18 years, history of cardiomyopathy, atrial fibrillation, coronary artery disease, moderate or greater valvular heart disease, or advanced liver disease. The control groups consisted of healthy volunteers whom underwent same-day CMRI and echocardiography as described in previous study.<sup>15</sup> All control subjects had no known history of cardiopulmonary disease. The study was approved by Institutional Review Board approved protocol with the informed consent obtained in all subjects.

## CMRI

CMR protocol along with the 4D-Flow MRI sequence was conducted as described previously.<sup>15,16</sup> Briefly, the CMR acquisition was acquired using a 1.5-T MRI Siemens system (MAGNETOM; Avanto) with an 8-channel phased array coil. A standard cine balanced SSFP technique with retrospective gating using end-respiratory breath holds was applied to generate short-axis images along the long axis in 8-mm increments as well as 4-chamber and 2-chamber views. Ventricular volumetric and functional analyses were performed using a standard contour based post-processing using commercially available software (Circle CVI 42, Calgary).

4D-Flow MRI sequence with prospective electrocardiogram gating, and respiratory navigators using bellows was applied to yield the field of view covering the entire mediastinum and great vessels. The typical scanning parameters were as follows: spatial resolution, 2.4–2.6 × 2.4–2.6 × 3.0 mm; alpha angle = 14° to 15°;

echo time/repetition time, 2.85/48.56 ms, velocity encoding 100–150 cm.s<sup>-1</sup> (adjusted per scouting images to avoid aliasing artifact). This approach yielded 14–19 cardiac phases with the final temporal resolution between 35 and 42. Resulting acquisition time varied based on heart rate and respiratory gating efficiency from 20 to 25 min.

## Vorticity calculation

Intracardiac vorticity calculation protocol confined to the RV cavity was applied as described previously.<sup>10,13,15</sup> Raw 4D-Flow MRI datasets were first pre-processed using denoising, anti-aliasing, and eddy-current corrections per consensus protocol.<sup>17</sup> The pre-processed files were then converted into case file for further quantitative analysis and flow visualization using open-source platform (Paraview, 5.11.0 or higher, Kitware). The final calculation steps are graphically depicted in Figure 1. Within the software platform, vorticity was calculated as a spatial derivative of the velocity vector field standardly as the cross product of the del operator and velocity vector field. Calculated vorticity magnitude was thereafter spatially integrated over the delineated RV cavity defined by the endocardial contours from 4D-Flow MRI magnitude images or superimposed SSFP images. Peak E (early filling) and A (atrial systole) phase vorticity values were then sampled from the vorticity waveform in each patient.

## Echocardiography

All subjects underwent standard Doppler and tissue Doppler imaging using a Vivid 7 ultrasound system (General Electric Medical Systems). The RV diastolic dysfunction was assessed and graded per the American Society of Echocardiography consensus-based recommendations.<sup>18</sup> Standard early filling (E) and atrial phase (A) Doppler velocities and their ratio (E/A) were recorded in each patient. Diastolic e' (early) and a' (late) velocities were obtained with pulsed tissue Doppler for the lateral tricuspid valve annulus. RV isovolumic relaxation time was also measured via Doppler tracings.

## Statistical analysis

All statistical analyses and data presentation were performed with Prism (version 9.0 or higher; GraphPad Software Inc). Variables were checked for the Gaussian distribution using normal plots and using D'Agostino

–Pearson, Shapiro–Wilk, and Kolmogorov–Smirnov tests. Variables that were skewed were natural log transformed, and skewed variables that included negative values were natural log-modulus transformed for correlative analyses. Baseline demographic and clinical variables were reported as mean or median values with corresponding standard deviation or interquartile range, respectively, as dictated by the data distribution. Inter-group comparisons were performed using unpaired 2-tailed t-test for normally distributed continuous variables or Mann–Whitney test for non-normally distributed variables, and  $\chi^2$  or Fisher exact test for categorical variables. The comparative analysis between the PAH, CLD-PH, and control groups was done using either 1-one way ANOVA or Kruskal–Wallis as dictated by the Gaussian distribution. Tukey's correction for multiple comparison's was applied for intergroup comparisons. The relationship between vorticity values and CMRI by simple linear regression analysis using the Pearson R value. Performed analyses were considered exploratory and hypothesis generating and adjustments for multiple comparisons were not employed. All performed tests were 2-sided and significance was based on an  $\alpha$ -level of  $\leq 0.05$ .

## RESULTS

In total 13 patients with PAH, 15 patients with PH-CLD, and 10 control subjects underwent the 4D-Flow MRI protocol. Patient demographics, RHC hemodynamics, and CMRI hemodynamics are summarized in Table 1. The spectrum of lung diseases within PH-CLD consisted from chronic obstructive pulmonary disease ( $n = 9$ ), interstitial lung fibrosis ( $n = 3$ ), and mixed emphysematous disease with pulmonary fibrosis ( $n = 3$ ). The median time between RHC and 4D-Flow MRI was 4 months (range: 0–9 months) and the median time between echocardiography and 4D-Flow MRI was 2 months (range: 0–5 months). Patients with PAH demonstrated increased mPAP when compared to PH-CLD ( $44 \pm 14$  vs.  $32 \pm 4$  mmHg,  $p = 0.012$ ) and increased pulmonary vascular resistance ( $13.3 \pm 7.9$  vs.  $5.2 \pm 1.8$  Wood's units,  $p = 0.007$ ). There were no differences in pulmonary arterial wedge pressure.

## CMRI

RV end-diastolic volume was increased in the PAH group when compared to controls (PAH vs. control:  $149 \pm 33$  vs.  $113 \pm 29$  mL,  $p = 0.003$ ). A similar relationship was observed between PH-CLD and control

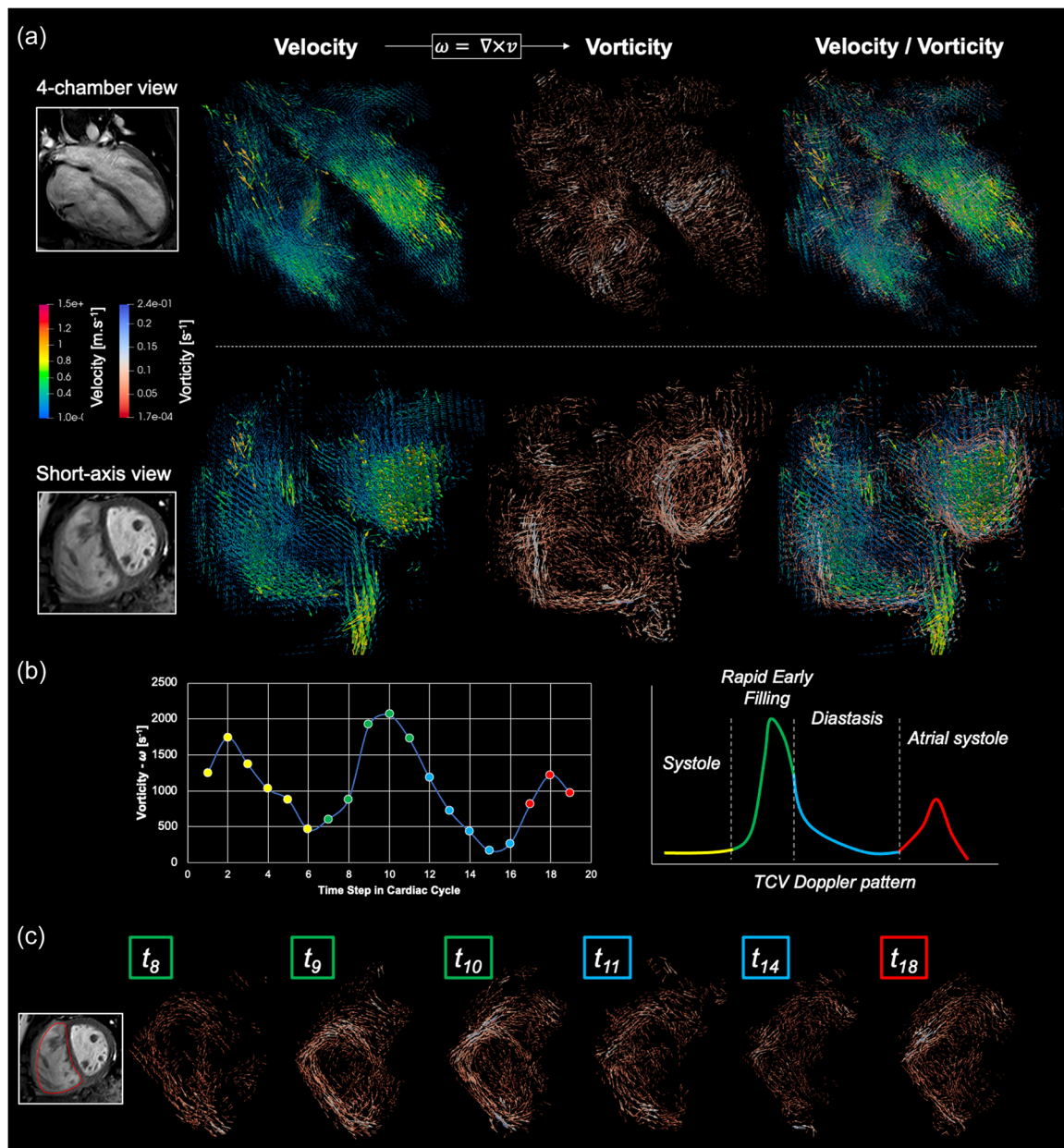


**FIGURE 1** The post-processing workflow of the right ventricular diastolic vorticity. (a) From the 4-chamber view and short-axis view perspectives, vector glyph represented velocity ( $v$ ) and vorticity ( $\omega$ ) vector fields for both left and right ventricles are visualized during early filling phase. (b) Calculated right ventricular vorticity throughout the cardiac cycle, with the corresponding tricuspid valve Doppler pattern. Individual color-coded data points represent a specific cardiac cycle phase: yellow = systole, green = rapid early filling phase, blue = diastasis, red = atrial systole. (c) From the short-axis view perspective, vorticity vector field segmented within the right ventricle during diastole with the time steps corresponding to the cardiac phases depicted in the above vorticity waveform.

groups (PH-CLD vs. control:  $155 \pm 36$  vs.  $113 \pm 29$  mL,  $p = 0.011$ ). There was no difference in end-diastolic volume values between PAH and PH-CLD groups ( $p = 0.618$ ). Similarly, when compared with the control group, end-systolic volumes were increased in both PAH (PAH vs. control:  $89 \pm 39$  vs.  $46 \pm 15$  mL,  $p < 0.001$ ) and PH-CLD groups (PAH vs. control:  $84 \pm 28$  vs.  $46 \pm 15$  mL,  $p < 0.001$ ). There was no difference in end-systolic volume between PAH and

PH-CLD groups ( $p = 0.692$ ). When compared to the control group, RV ejection fraction was reduced in both PAH patients (PAH vs. control:  $42 \pm 14$  vs.  $60 \pm 6$  mL,  $p < 0.001$ ) and PH-CLD patients (PAH vs. control:  $46 \pm 11$  vs.  $60 \pm 6$  mL,  $p < 0.001$ ). There was no difference in RV ejection fraction between PAH and PH-CLD groups ( $p = 0.515$ ). Finally, no differences were observed between the considered groups in stroke volume, cardiac output, and heart rate.

**TABLE 1** Patient characteristics and standard cardiac MRI hemodynamics.

	PAH (N = 13)	CLD-PAH (N = 15)	Control (N = 10)	p Value
Age (years)	60.2 ± 7.6	63.3 ± 8.7	57.7 ± 9.2	0.296
Sex (Female)	2 (15%)	7 (47%)	3 (30%)	0.205
BSA (kg/m <sup>2</sup> )	1.74 ± 0.24	1.81 ± 0.27	1.87 ± 0.25	0.650
<i>Catheterization hemodynamics</i>				
mPAP (mmHg)	44 ± 14	32 ± 4		0.014
PVR (WU)	13.3 ± 7.9	5.2 ± 1.8		0.007
PAWP (mmHg)	13 ± 5	11 ± 4		0.176
RAP (mmHg)	8 ± 4	7 ± 3		0.394
<b>Cardiac MRI</b>				
RV EDV (mL)	149 ± 33*	155 ± 36*	113 ± 29	0.013
RV ESV (mL)	89 ± 39*	84 ± 28**	46 ± 15	0.002
RV SV (mL)	59 ± 13	71 ± 25	67 ± 17	0.299
RVEF (%)	42 ± 14**	46 ± 11**	60 ± 6	0.002
CO (L/min)	3.7 ± 1.3	3.5 ± 1.7	3.8 ± 0.8	0.408
Heart rate (bpm)	62 ± 19	50 ± 17	57 ± 7	0.230

Note: Data reported as mean ± SD. Reported p Value is either unpaired t-test or one way ANOVA.

Abbreviations: BSA, body surface area; CO, cardiac output; EDV, end-diastolic volume; EF, ejection fraction; ESV, end-systolic volume; mPAP, mean pulmonary arterial pressure; PAWP, pulmonary arterial wedge pressure; PVR, pulmonary vascular resistance; RV, right ventricle; SV, stroke volume.

\*p < 0.05 from control group; \*\*p < 0.01 from control group.

## RV diastolic dysfunction

Echocardiographic and 4D-Flow MRI derived biomarkers of RV diastolic dysfunction are summarized in Table 2 and intergroup comparison of the critical imaging variables is graphically displayed in Figure 2. Standard spectral Doppler E velocity was no different between the considered groups, but Doppler A velocity was increased in PAH group when compared to control group (PAH vs. control: 42 ± 10 vs. 26 ± 8 cm.s<sup>-1</sup>, p < 0.001) and also increased in PH-CLD group (PH-CLD vs. control: 42 ± 8 vs. 26 ± 8 cm.s<sup>-1</sup>, p < 0.001). There was no difference in Doppler A velocity between the PAH and PH-CLD group (p = 0.942). Correspondingly, the E/A ratio was decreased in PAH (PAH vs. control: 1.0 ± 0.3 vs. 1.8 ± 0.6, p < 0.001) and in PH-CLD (PH-CLD vs. control: 1.0 ± 0.5 vs. 1.8 ± 0.6, p < 0.001). However, there was no difference in E/A ratio between the two PH groups (p = 0.884). Tissue Doppler e' velocity was decreased in PAH when compared to controls (PAH vs. control: 7 ± 2 vs. 14 ± 4 cm.s<sup>-1</sup>, p < 0.001) and similarly in PH-CLD (PH-CLD vs. control: 6 ± 1 vs. 14 ± 4 cm.s<sup>-1</sup>, p < 0.001). No difference was observed in e' velocity between PAH and PH-CLD groups (p = 0.531). The E/e' ratio was increased in PAH (PAH vs. control: 6.3 ± 1.8 vs. 3.4 ± 0.8, p < 0.001) and similarly in PH-CLD

(PH-CLD vs. control: 6.5 ± 2.3 vs. 3.4 ± 0.8, p < 0.001) with no observed difference between PAH and PH-CLD groups (p = 0.788). Lastly, there were no intergroup differences in tricuspid valve deceleration time.

Intergroup comparison of the 4D-Flow MRI derived vorticity values is summarized in Table 2. Considering the early filling E-vorticity, significance intergroup differences were observed between each considered group. Patients with PAH had the lowest E-vorticity observed when compared to both control group (PAH vs. Control: 1954 ± 829 vs. 4507 ± 837 s<sup>-1</sup>, p < 0.001) and PH-CLD group (1954 ± 829 vs. 3110 ± 890 s<sup>-1</sup>, p = 0.045). Furthermore, patients with PH-CLD had lower E-vorticity compared to controls (3110 ± 890 vs. 4507 ± 837 s<sup>-1</sup>, p = 0.026). The control group had also increased median atrial filling phase A-vorticity when compared to PAH (p = 0.012). Lastly, median value of the vorticity-based E/A ratio was increased in control group when compared to both PAH (p < 0.001) and PH-CLD (p = 0.002) groups.

Representative examples of visualized vorticity vector field from the short-axis view perspective are portrayed in Figure 3. The overall magnitude of the vorticity vector field was observed to be higher throughout diastole in control patients when compared to both PAH and PH-CLD group. In all groups vorticity is generated primary

**TABLE 2** Right ventricular diastolic dysfunction—echocardiography and 4D-Flow MRI.

	PAH (N = 13)	CLD-PAH (N = 15)	Control (N = 10)	p Value
<i>Echocardiography</i>				
E (cm.s <sup>-1</sup> )	42 ± 13	41 ± 14	43 ± 8	0.732
A (cm.s <sup>-1</sup> )	42 ± 10**	42 ± 8**	26 ± 8	<0.001
E/A	1.0 ± 0.3**	1.0 ± 0.5**	1.8 ± 0.6	0.001
e' (cm.s <sup>-1</sup> )	7 ± 2**	6 ± 1**	14 ± 4	<0.001
a' (cm.s <sup>-1</sup> )	14 ± 4	15 ± 4	13 ± 3	0.499
E/e'	6.3 ± 1.8**	6.5 ± 2.3**	3.4 ± 0.8	<0.001
TVDT (ms)	229 ± 46	305 ± 60	265 ± 92	0.108
<i>4D-Flow MRI</i>				
E-wave vorticity (s <sup>-1</sup> )	1954 ± 829,** <sup>+</sup>	3110 ± 890**	4507 ± 837	<0.001
A-wave vorticity (s <sup>-1</sup> )	321 (245–1934)	177 (149–302)*	1073 (319–1693)	0.012
E/A vorticity	2.7 (1.8–10.6)	5.3 (0.7–9.0)	24.5 (17.4–28.3)	<0.001

Note: Data reported as mean ± SD or median with corresponding IQR.

Abbreviations: A, atrial phase Doppler velocity; a', late phase right ventricular free wall tissue Doppler velocity; CLD-PH, pulmonary hypertension associated with chronic lung disease; E, early filling Doppler velocity, e', early right ventricular free wall tissue Doppler velocity, PAH, pulmonary arterial hypertension; TVDT, tricuspid velocity deceleration time.

\*p < 0.05 from Control;

\*\*<0.01 from Control, +<0.05 from CLD-PAH.

along the RV cavity and most prominently close to the tricuspid valve annulus where the velocity gradient is the highest. In comparison to PH groups, control patients additionally demonstrated a source of vorticity in the centrally in the RV cavity and in the RV outflow tract.

### Relationship between RV vorticity and CMRI indices

To further explore the relationship between RV inflow characteristics and RV size/function, we subjected the RV E-vorticity to linear regression with standard CMRI hemodynamics and echocardiographic Doppler characteristic. The summary of evaluated correlations is depicted in Table 3 and strongest correlations are graphically depicted in Figure 4. E-vorticity correlated with ejection fraction ( $R = 0.60$ ,  $p < 0.001$ ), end-systolic volume ( $R = 0.50$ ,  $p = 0.001$ ), stroke volume ( $R = 0.42$ ,  $p = 0.007$ ), and cardiac output ( $R = 0.30$ ,  $p = 0.027$ ). No correlations were observed between E-vorticity and end-diastolic volume. RV-vorticity was also associated with the Doppler E/A ratio ( $R = 0.43$ ,  $p = 0.006$ ), e' velocity ( $R = 0.53$ ,  $p < 0.001$ ), and E/e' ratio ( $R = 0.35$ ,  $p = 0.027$ ). There was no association between E-vorticity and spectral Doppler E velocity.

### DISCUSSION

RV diastolic dysfunction is a critical pathologic consequence of RV remodeling during PH progression with important clinical and functional predictive value.<sup>19–22</sup> Signs of impaired RV filling measured by standard echocardiography or RHC have been previously reported across the entire PH spectrum.<sup>23–25</sup> However, typical spectral Doppler measurements of diastolic dysfunction are influenced by heart rate and loading conditions, introducing interpretation variability into this diagnostic modality.<sup>26,27</sup> Consequently, impaired filling and RV diastolic stiffness needs to be interpreted in the context of the RV afterload. The present study demonstrates that 4D-Flow MRI derived vorticity can differentiate abnormal RV filling hemodynamics between PAH and PH-CLD patients with (1) similar spectral Doppler and tissue Doppler characteristics, (2) similar degree of geometric RV remodeling, and (3) different loading condition. Our results add to the increasing body of evidence suggesting that intracardiac flow characterization might serve as early and sensitive marker of diastolic dysfunction.<sup>7,28</sup>

Diastolic dysfunction is a multifactorial process manifested by pathologic changes on the cardiomyocyte level resulting in loss of restoration forces within the sarcomeric apparatus and by the intrinsic remodeling of myocardial

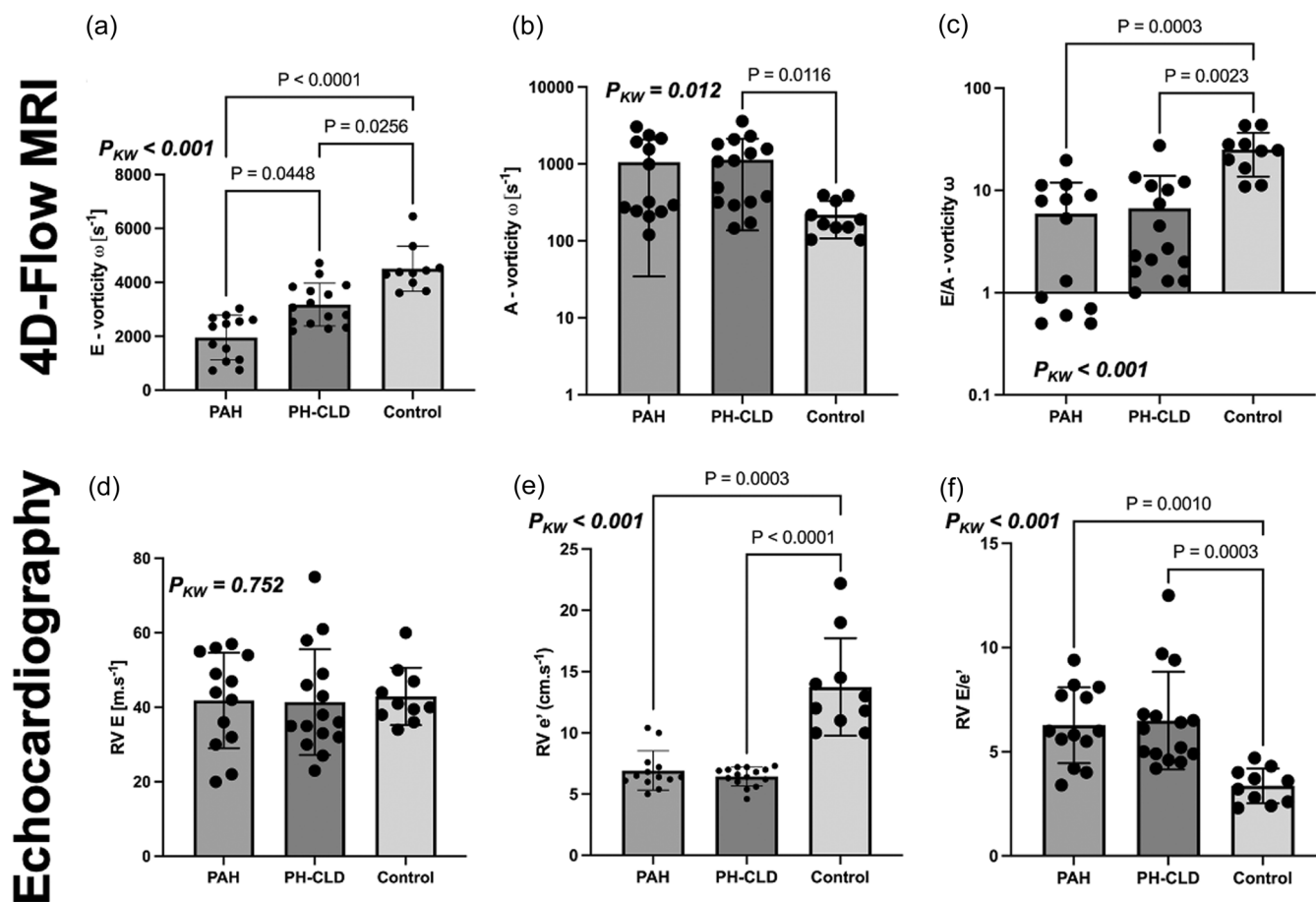


**FIGURE 2** Comparison of the right ventricular diastolic dysfunction imaging biomarkers between pulmonary arterial hypertension (PAH) and pulmonary hypertension due to chronic lung disease (PH-CLD) and control groups. (a) 4D-Flow MRI derived E-vorticity was the only discriminating biomarker differentiating all groups with the lowest E-vorticity values noted in PAH patients. (b) Atrial phase A-vorticity was no different between the PAH and PH-CLD groups yet both PH groups has increased A-vorticity when compared to control group. (c) Similar findings were observed for the E/A vorticity ratio. (d) There were no differences in Doppler E-wave velocity between the considered group. (e) Tissue Doppler  $e'$  velocity was decreased in both PH groups when compared to controls with no differences between the specific PH groups. (f) Similarly,  $E/e'$  ratio was increased in both PH groups but there were no differences between specific PH groups.

extracellular matrix leading to mechanically impaired ventricular relaxation.<sup>29</sup> Cumulatively this results in increased diastolic stiffness or reduced ventricular elastance compromising preload generation. In PH, the intrinsic structural changes in myocardial tissue have been demonstrated by increased collagen deposition within the extracellular matrix and at the level of cardiomyocyte level by reduced titin phosphorylation leading to increased passive tension of sarcomeric units.<sup>30</sup> The ideal load-independent and current gold standard approach for accurate evaluation of the RV diastolic stiffness in research is by means of pressure-volume loop analysis and calculation of the end-diastolic ventricular elastance and isovolumic relaxation time constant  $\tau$ .<sup>31</sup> This approach is ideal for initial RHC characterization but, as an invasive diagnostic, is less optimal for screening and sequential follow-up. Consequently, noninvasive imaging methods have been employed

to characterize RV diastolic dysfunction and RV stiffness by means of myocardial deformation analysis.<sup>32</sup>

Multiple CMRI tissue mapping studies have reported on structural myocardial changes in PH patients demonstrating increased extracellular volume and fibrotic changes in RV myocardium but its association to diastolic stiffness is yet to be determined.<sup>33–35</sup> With regard to 4D-Flow MRI, RV diastolic dysfunction has been interrogated previously using multiple parameters including vorticity, 4-flow component analysis, and kinetic energy.<sup>25,36–39</sup> With the goal to replace qualitative vortex grading strategies, vorticity has emerged as an ideal marker for inflow characterization in morphologically complex RV.<sup>15,40,41</sup> In this study, early filling phase E-vorticity was the only variable distinguishing PAH and PH-CLD cohorts. Vorticity is primarily generated along the endocardial surfaces where the spatial velocity

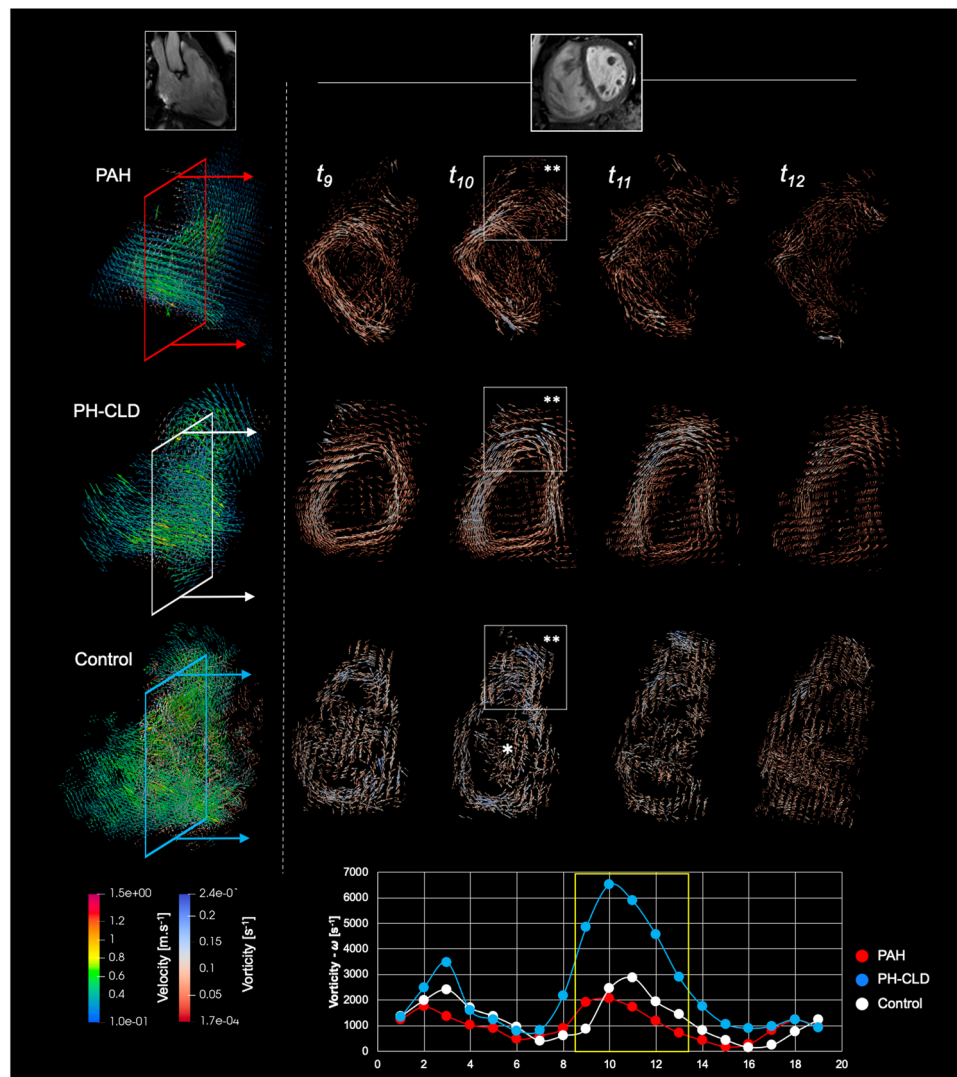


**FIGURE 3** Comparison of the right ventricular (RV) velocity and vorticity vector fields in representative patients with pulmonary arterial hypertension (PAH), pulmonary hypertension due to chronic lung disease (PH-CLD), and control subject. The most left column depicts velocity vector field with the superimposed vorticity field oriented from the right long axis - RV outflow tract view. Other columns depicts intracardiac vorticity from the short-axis view perspective during early diastolic filling phase. Vorticity is in each subject generated primarily along the endocardial surfaces. One can appreciate higher density and magnitude of vorticity vector glyphs in the control subject with additional source of vorticity generated within the RV outflow tract (\*\*) and inside the RV cavity (\*). Representative RV vorticity waveforms through the cardiac cycle are depicted at the bottom of the figure.

gradient reaches the maximum. Interestingly, E-vorticity values were not associated with RV end-diastolic volume and Doppler E wave velocities suggesting that additional flow kinematic interactions beyond RV surface geometry and velocity might play role in diastolic filling. Similar to previous results, E-vorticity was associated with RV tissue Doppler  $e'$  values suggesting that the degree of RV elastic recoil might play a critical role in vorticity generation.<sup>10,15</sup> Another distinguishing feature observed in this study was a lack of vorticity generation in PH groups in the RV outflow tract. Upon passing tricuspid valve, a substantive portion of the RV inflow is redirected

toward the outflow tract where the conical geometry creates an ideal substrate for vorticity generation. We hypothesize that combination of compromised RV recoil and RV dilation might disable high velocity flow to the RV outflow tract.

Abnormal echocardiographic markers of RV diastolic dysfunction have been previously reported in both PAH and PH-CLD patient groups but there is a lack comparative studies between these groups.<sup>5,42</sup> In this study RV vorticity was different between the two groups despite similar RV ejection fraction and the degree of RV dilation. Expectedly, the primary distinguishing feature



of the two groups was the severity of PH with significantly higher mPAPs in PAH group. Whether the cause of further reduction in vorticity in PAH patients is primarily due to afterload and/or more severe diastolic dysfunction is yet to be determined. However, compromised RV diastolic dysfunction can contribute to ventilatory and circulatory exercise limitation and symptomatology in both patient groups.<sup>3,22</sup> In future studies we will consider combining pressure-volume analysis with the CMRI to study the end-diastolic RV elastance in the context of RV flow formations.

## Limitations

We would like to acknowledge several limitations pertinent to this study. Firstly, this was a single

institution study and therefore results are prone to patient selection bias, particularly when selecting patients with more severe grade of PH. Secondly, echocardiography and RHC were not temporally aligned with the 4D-Flow MRI acquisition. In future studies we plan on investigating pressure hemodynamic derived variables to yield markers of RV diastolic dysfunction (RV  $\tau$  constant) and RV diastolic stiffness (RV end-diastolic elastance), and correlate these variables with 4D-Flow MRI vorticity and 4-flow component data. Finally, the major limitation of 4D-Flow MRI remains to be a low temporal resolution which might result in sampling error and potentially underestimation of the peak diastolic vorticity values.

## CONCLUSIONS

Here we present a single institution comparison of CMR intracavitary RV flow characteristics and standard echocardiographic assessment in the setting of PAH and PH-CLD. Importantly, we demonstrate increased discrimination in imaging markers of RV diastolic dysfunction between PH subtypes by 4D-Flow MRI compared with echocardiography in this adult cohort. These data demonstrate that 4D-Flow MRI may be beneficial as a noninvasive diagnostic tool to differentiate the disease phenotypes more accurately than standard echocardiography. Further characterization of flow patterns and detailed definition of unique flow characteristics across all PH subtypes will be critical to better define the role of 4D-Flow MRI as clinically prognostic tool in adult PH.

## AUTHOR CONTRIBUTIONS

Michael Cain, Michal Schafer, Jordan Hoffman, and Brett Fenster made substantial contributions to the conception and design of the work. Data were analyzed

**TABLE 3** Correlations between RV E-vorticity and RV hemodynamic MRI/Echo indices.

	Beta $\pm$ SE	R Value	p Value
Ejection fraction	0.006 $\pm$ 0.001	0.60	<0.001
End-diastolic volume	-0.007 $\pm$ 0.005	0.24	0.147
End-systolic volume	-0.013 $\pm$ 0.004	0.50	0.001
Stroke volume	0.006 $\pm$ 0.002	0.42	0.007
Heart rate	0.001 $\pm$ 0.002	0.10	0.657
Cardiac output	0.04 $\pm$ 0.02 <sup>a</sup>	0.30	0.027
Doppler E	0.03 $\pm$ 0.015 <sup>a</sup>	0.00	0.983
Doppler E/A	0.018 $\pm$ 0.006 <sup>a</sup>	0.43	0.006
Tissue Doppler e'	0.015 $\pm$ 0.04 <sup>a</sup>	0.53	<0.001
E/e'	0.06 $\pm$ 0.03 <sup>a</sup>	0.35	0.027

Note: Data reported as beta coefficient  $\pm$  standard error with corresponding Pearson R Value and p Value.

<sup>a</sup>Beta and SE value are multiplied by 103.

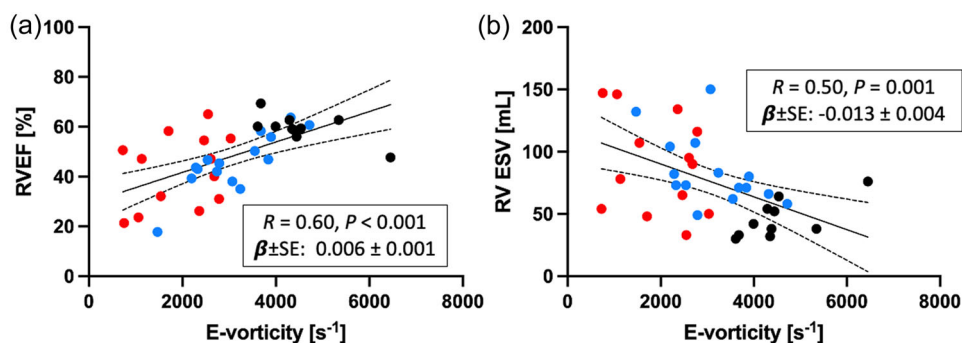


**FIGURE 4** Graphical representation of the most significant correlations showing the relationship between the 4D-Flow MRI vorticity and (a) right ventricular ejection fraction (RVEF) and (b) RV end-systolic volume (RV-ESV).

by Michael Cain, Michal Schafer, and Lexie Ross. Michal Schafer and Alex Barker were responsible for the statistical analysis. Dunbar Ivy, Todd Bull, Lexie Ross Brett Fenster, and Daniel Vargas contributed to the interpretation of the data. All authors contributed to drafting and revising of the article. Michal Schafer and Michael Cain have accessed and verified the data. Dunbar Ivy and Jordan Hoffman provided overall supervisory support and approved the final version of the manuscript.

### ACKNOWLEDGMENTS

This work was supported by Rady Family and Jayden DeLuca foundations.

### CONFLICT OF INTEREST STATEMENT

The authors declare no conflict of interest.

### ETHICS STATEMENT

The study was approved by the Institutional Review Board approved protocol with the informed consent obtained in all subjects and all study procedures were performed in accordance with the ethical standards of the Helsinki Declaration.

### ORCID

Michael T. Cain  <http://orcid.org/0000-0003-4029-2557>  
Michal Schäfer  <http://orcid.org/0000-0002-1794-3262>

### REFERENCES

- Seeger W, Adir Y, Barberà JA, Champion H, Coghlan JG, Cottin V, De Marco T, Galiè N, Ghio S, Gibbs S, Martinez FJ, Semigran MJ, Simonneau G, Wells AU, Vachiéry JL. Pulmonary hypertension in chronic lung diseases. *JACC*. 2013; 62(25 SUPPL.):D109–16.
- Chaouat A, Naeije R, Weitzenblum E. Pulmonary hypertension in COPD. *Eur Respir J*. 2008;32:1371–85.
- Humbert M, Kovacs G, Hoeper MM, Badagliacca R, Berger RMF, Brida M, Carlsen J, Coats AJS, Escribano-Subias P, Ferrari P, Ferreira DS, Ghofrani HA, Giannakoulas G, Kiely DG, Mayer E, Meszaros G, Nagavci B, Olsson KM, Pepke-Zaba J, Quint JK, Rådegran G, Simonneau G, Sitbon O, Tonia T, Toshner M, Vachiery JL, Vonk Noordegraaf A, Delcroix M, Rosenkranz S, Schwerzmann M, Dinh-Xuan AT, Bush A, Abdelhamid M, Aboyans V, Arbustini E, Asteggiano R, Barberà JA, Beghetti M, Čelutkienė J, Cikes M, Condliffe R, de Man F, Falk V, Fauchier L, Gaine S, Galiè N, Gin-Sing W, Granton J, Grünig E, Hassoun PM, Hellemons M, Jaarsma T, Kjellström B, Klok FA, Konradi A, Koskinas KC, Kotecha D, Lang I, Lewis BS, Linhart A, Lip GYH, Løchen ML, Mathioudakis AG, Mindham R, Moledina S, Naeije R, Nielsen JC, Olschewski H, Opitz I, Petersen SE, Prescott E, Rakisheva A, Reis A, Ristić AD, Roche N, Rodrigues R, Selton-Suty C, Souza R, Swift AJ, Touyz RM, Ulrich S, Wilkins MR, Wort SJ. 2022 ESC/ERS guidelines for the diagnosis and treatment of pulmonary hypertension. *Eur Heart J*. 2022;43: 3618–731.
- Vonk Noordegraaf A, Westerhof BE, Westerhof N. The relationship between the right ventricle and its load in pulmonary hypertension. *JACC*. 2017;69:236–43.
- Kiely DG, Levin DL, Hassoun PM. Statement on imaging and pulmonary hypertension from the pulmonary vascular research institute (PVRI). *Pulm Circ*. 2019;9(3):1–32.
- Cerne JW, Pathrose A, Gordon DZ, Sarnari R, Veer M, Blaisdell J, Allen BD, Avery R, Markl M, Ragin A, Carr JC. Evaluation of pulmonary hypertension using 4D flow MRI. *J Magn Reson Imaging*. 2022;56:234–45.
- Pedrizetti G, La Canna G, Alfieri O, Tonti G. The vortex--an early predictor of cardiovascular outcome? *Nat Rev Cardiol*. 2014;11:545–53.
- Ashkir Z, Myerson S, Neubauer S, Carlhäll CJ, Ebberts T, Raman B. Four-dimensional flow cardiac magnetic resonance assessment of left ventricular diastolic function. *Front Cardiovasc Med*. 2022;9:1942.
- Eriksson J, Bolger AF, Ebberts T, Carlhäll CJ. Four-dimensional blood flow-specific markers of LV dysfunction in dilated cardiomyopathy. *Eur Heart J Cardiovasc Imaging*. 2013;14:417–24.
- Schäfer M, Browning J, Schroeder JD, Shandas R, Kheyfets VO, Buckner JK, Hunter KS, Hertzberg JR, Fenster BE. Vorticity is a marker of diastolic ventricular interdependency in pulmonary hypertension. *Pulm Circ*. 2016;6:46–54.
- Stoll VM, Hess AT, Rodgers CT, Bissell MM, Dyverfeldt P, Ebberts T, Myerson SG, Carlhäll CJ, Neubauer S. Left ventricular flow analysis. *Circ Cardiovasc Imag*. 2019;12:1–12.
- Ramos JG, Fyrdahl A, Wieslander B. Cardiovascular magnetic resonance 4D flow analysis has a higher diagnostic yield than Doppler echocardiography for detecting increased pulmonary artery pressure. *BMC Med Genet*. 2020;21:1–9.
- Schäfer M, Humphries S, Stenmark KR, Kheyfets VO, Buckner JK, Hunter KS, Fenster BE. 4D-flow cardiac magnetic resonance-derived vorticity is sensitive marker of left ventricular diastolic dysfunction in patients with mild-to-moderate chronic obstructive pulmonary disease. *Eur Heart J Cardiovasc Imaging*. 2018;19:415–24.
- Schäfer M, Barker AJ, Kheyfets V, Stenmark KR, Crapo J, Yeager ME, Truong U, Buckner JK, Fenster BE, Hunter KS. Helicity and vorticity of pulmonary arterial flow in patients with pulmonary hypertension: quantitative analysis of flow formations. *J Am Heart Assoc*. 2017;6:e007010.
- Fenster BE, Browning J, Schroeder JD. Vorticity is a marker of right ventricular diastolic dysfunction. *Am J Physiol - Hear Circ Physiol*. 2015;309:H1087–93.
- Schäfer M, Barker AJ, Kheyfets V. Helicity and vorticity of pulmonary arterial flow in patients with pulmonary hypertension: quantitative analysis of flow formations. *J Am Heart Assoc*. 2017;6(12):e007010.
- Dyverfeldt P, Bissell M, Barker AJ, Bolger AF, Carlhäll CJ, Ebberts T, Francios CJ, Frydrychowicz A, Geiger J, Giese D, Hope MD, Kilner PJ, Kozerke S, Myerson S, Neubauer S, Wieben O, Markl M. 4D flow cardiovascular magnetic resonance consensus statement. *J Cardiovasc Magn Reson*. 2015;17:72.

18. Rudski LG, Lai WW, Afilalo J, Hua L, Handschumacher MD, Chandrasekaran K, Solomon SD, Louie EK, Schiller NB. Guidelines for the echocardiographic assessment of the right heart in adults: A report from the American society of echocardiography. *J Am Soc Echocardiogr.* 2010;23:685–713.
19. Bernardo RJ, Haddad F, Couture EJ, Hansmann G, Perez VAJ, Denault AY, Man FS, Amsallem M. Mechanics of right ventricular dysfunction in pulmonary arterial hypertension and heart failure with preserved ejection fraction. *Cardiovasc Diagn Ther.* 2020;10:1580–603.
20. Trip P, Rain S, Handoko ML, van der Bruggen C, Bogaard HJ, Marcus JT, Boonstra A, Westerhof N, Vonk-Noordegraaf A, de Man FS. Clinical relevance of right ventricular diastolic stiffness in pulmonary hypertension. *Eur Respir J.* 2015;45:1603–12.
21. Vanderpool RR, Pinsky MR, Naeije R, Deible C, Kosaraju V, Bunner C, Mathier MA, Lacomis J, Champion HC, Simon MA. RV-pulmonary arterial coupling predicts outcome in patients referred for pulmonary hypertension. *Heart.* 2015;101:37–43.
22. Tello K, Dalmer A, Vanderpool R, Ghofrani HA, Naeije R, Roller F, Seeger W, Dumitrescu D, Sommer N, Brunst A, Gall H, Richter MJ. Impaired right ventricular lusitropy is associated with ventilatory inefficiency in pulmonary arterial hypertension. *Eur Respir J.* 2019;54:1900342.
23. Gan CTJ, Holverda S, Marcus JT, Paulus WJ, Marques KM, Bronzwaer JGF, Twisk JW, Boonstra A, Postmus PE, Vonk-Noordegraaf A. Right ventricular diastolic dysfunction and the acute effects of sildenafil in pulmonary hypertension patients. *Chest.* 2007;132:11–7.
24. Fenster BE, Holm KE, Weinberger HD, Moreau KL, Meschede K, Crapo JD, Make BJ, Bowler R, Wamboldt FS, Hoth KF. Right ventricular diastolic function and exercise capacity in COPD. *Respir Med.* 2015;109:1287–92.
25. Schäfer M, Frank BS, Ivy DD, Abman SH, Stenmark KR, Mitchell MB, Browne LP, Barker AJ, Hunter KS, Kheifets V, Miller-Reed K, Ing R, Morgan GJ, Truong U. Short-Term effects of inhaled nitric oxide on right ventricular flow hemodynamics by 4-Dimensional-Flow magnetic resonance imaging in children with pulmonary arterial hypertension. *J Am Heart Assoc.* 2021;10:e020548.
26. Mauritz G-J, Vonk-Noordegraaf A, Kind T, Surie S, Kloek JJ, Bresser P, Saouti N, Bosboom J, Westerhof N, Marcus JT. Pulmonary endarterectomy normalizes interventricular dyssynchrony and right ventricular systolic wall stress. *J Cardiovasc Magn Reson.* 2012;14:5.
27. Nagueh SF, Smiseth OA, Appleton CP, Byrd BF, Dokainish H, Edvardsen T, Flachskampf FA, Gillebert TC, Klein AL, Lancellotti P, Marino P, Oh JK, Popescu BA, Waggoner AD. Recommendations for the evaluation of left ventricular diastolic function by echocardiography: an update from the American society of echocardiography and the European association of cardiovascular imaging. *J Am Soc Echocardiogr.* 2016;29:277–314.
28. Arvidsson PM, Töger J, Pedrizzetti G, Heiberg E, Borgquist R, Carlsson M, Arheden H. Hemodynamic forces using four-dimensional flow MRI: an independent biomarker of cardiac function in heart failure with left ventricular dyssynchrony? *Am J Physiol Heart Circ Physiol.* 2018;315:H1627–39.
29. Flachskampf FA, Biering-Sørensen T, Solomon SD, Duvernoy O, Bjerner T, Smiseth OA. Cardiac imaging to evaluate left ventricular diastolic function. *JACC.* 2015;8:1071–93.
30. Rain S, Handoko ML, Trip P, Gan CTJ, Westerhof N, Stienen GJ, Paulus WJ, Ottenheim CAC, Marcus JT, Dorfmueller P, Guignabert C, Humbert M, MacDonald P, dos Remedios C, Postmus PE, Saripalli C, Hidalgo CG, Granzier HL, Vonk-Noordegraaf A, van der Velden J, de Man FS. Right ventricular diastolic impairment in patients with pulmonary arterial hypertension. *Circulation.* 2013;128(2016–25):2016–25.
31. Tello K, Dalmer A, Axmann J, Vanderpool R, Ghofrani HA, Naeije R, Roller F, Seeger W, Sommer N, Wilhelm J, Gall H, Richter MJ. Reserve of right Ventricular-Arterial coupling in the setting of chronic overload. *Circ: Heart Failure.* 2019;12:e005512.
32. Tello K, Dalmer A, Vanderpool R, Ghofrani HA, Naeije R, Roller F, Seeger W, Wilhelm J, Gall H, Richter MJ. Cardiac magnetic resonance Imaging-Based right ventricular strain analysis for assessment of coupling and diastolic function in pulmonary hypertension. *JACC Cardiovasc Imag.* 2019;12:2155–64.
33. Alabed S, Saunders L, Garg P, Shahin Y, Alandejani F, Rolf A, Puntmann VO, Nagel E, Wild JM, Kiely DG, Swift AJ. Myocardial T1-mapping and extracellular volume in pulmonary arterial hypertension: a systematic review and meta-analysis. *Magn Reson Imag.* 2021;79:66–75.
34. Swift AJ, Rajaram S, Capener D, Elliot C, Condliffe R, Wild JM, Kiely DG. LGE patterns in pulmonary hypertension do not impact overall mortality. *JACC: Cardiovasc Imag.* 2014;7:1209–17.
35. Freed BH, Gomberg-Maitland M, Chandra S, Mor-Avi V, Rich S, Archer SL, Jamison EB, Lang RM, Patel AR. Late gadolinium enhancement cardiovascular magnetic resonance predicts clinical worsening in patients with pulmonary hypertension. *J Cardiovasc Magn Reson.* 2012;14:11.
36. Fenster B, Podgorski CA, Schroeder JD, Lin B, Reisner SD, Browning J, Hertzberg JR, Buckner KJ, Schafer M. Left ventricular vorticity is marker of ventricular interdependency in pulmonary arterial hypertension. *J Cardiovasc Magn Reson.* 2015;17(Suppl 1):P14.
37. Zhao X, Leng S, Tan RS, Chai P, Yeo TJ, Bryant JA, Teo LLS, Fortier MV, Ruan W, Low TT, Ong CC, Zhang S, van der Geest RJ, Allen JC, Hughes M, Garg P, Tan TH, Yip JW, Tan JL, Zhong L. Right ventricular energetic biomarkers from 4D flow CMR are associated with exertional capacity in pulmonary arterial hypertension. *J Cardiovasc Magn Reson.* 2022;24:61.
38. Fredriksson AG, Svalbring E, Eriksson J, Dyverfeldt P, Alehagen U, Engvall J, Ebbers T, Carlhäll CJ. 4D flow MRI can detect subtle right ventricular dysfunction in primary left ventricular disease. *J Magn Reson Imaging.* 2016;43:558–65.
39. Fredriksson A, Trzebiatowska-Krzynska A, Dyverfeldt P, Engvall J, Ebbers T, Carlhäll CJ. Turbulent kinetic energy in the right ventricle: potential MR marker for risk stratification of adults with repaired tetralogy of fallot. *J Magn Reson Imaging.* 2018;47:1043–53.
40. Elsayed A, Mauger CA, Ferdian E, Gilbert K, Scadeng M, Occlshaw CJ, Lowe BS, McCulloch AD, Omens JH, Govil S,

- Pushparajah K, Young AA. Right ventricular flow vorticity relationships with biventricular shape in adult tetralogy of fallot. *Front Cardiovasc Med.* 2022;8:2221.
41. Loke YH, Capuano F, Cleveland V, Mandell JG, Balaras E, Olivieri LJ. Moving beyond size: vorticity and energy loss are correlated with right ventricular dysfunction and exercise intolerance in repaired tetralogy of fallot. *J Cardiovasc Magn Reson.* 2021;23:98.
  42. Kolb TM, Hassoun PM. Right ventricular dysfunction in chronic lung disease. *Cardiol Clin.* 2012;30:243–56.

**How to cite this article:** Cain MT, Schäfer M, Ross LK, Ivy DD, Mitchell MB, Fenster BE, Bull TM, Barker AJ, Vargas D, Hoffman JRH. 4D-Flow MRI intracardiac flow analysis considering different subtypes of pulmonary hypertension. *Pulm Circ.* 2023;13:e12307.  
<https://doi.org/10.1002/pul2.12307>